

Ultrastrong parametric coupling between a superconducting cavity and a mechanical resonator

G. A. Peterson,^{1,2} S. Kotler,^{1,2} F. Lecocq,^{1,2} K. Cicak,¹ X. Y. Jin,^{1,2} R. W. Simmonds,¹ J. Aumentado,¹ and J. D. Teufel¹

¹National Institute of Standards and Technology, 325 Broadway, Boulder, CO 80305, USA

²Department of Physics, University of Colorado, Boulder, CO 80309, USA

(Dated: June 28, 2019)

We present a new optomechanical device where the motion of a micromechanical membrane couples to a microwave resonance of a three-dimensional superconducting cavity. With this architecture, we realize ultrastrong parametric coupling, where the coupling rate not only exceeds the dissipation rates in the system but also rivals the mechanical frequency itself. In this regime, the optomechanical interaction induces a frequency splitting between the hybridized normal modes that reaches 88% of the bare mechanical frequency, limited by the fundamental parametric instability. The coupling also exceeds the mechanical thermal decoherence rate, enabling new applications in ultrafast quantum state transfer and entanglement generation.

Keywords: cavity optomechanics, superconducting circuits, ultrastrong coupling

The physics of coupled oscillators is used to understand a wide array of natural and man-made phenomena, from the microscopic vibrations of atoms and molecules to the interplay of planets and their moons. Coupling strengths can be grouped into different regimes that entail qualitatively different behavior. In particular, the regimes of weak and strong coupling are distinguished by whether or not the coupling between two oscillators exceeds their damping rates. In the strong coupling regime, the eigenfrequencies of the combined system split into normal modes where the energy swaps back and forth between the individual oscillators. For low-loss systems, this energy exchange can be fast compared to the lifetimes of the individual modes while still remaining slow compared to their periods. The strong coupling regime has become an essential tool in engineered quantum systems because it can allow the subsystems to exchange their quantum information before it is lost due to decoherence [1]. As quantum devices continue to be engineered with increased coupling rates, a new regime known as ultrastrong coupling has become relevant. This regime occurs once the coupling rate becomes so large as to rival a bare resonance frequency, resulting in new quantum effects including multimode entanglement and virtually excited ground states [2, 3]. Reaching ultrastrong coupling and studying its effect in quantum devices remains an active experimental challenge.

Cavity optomechanics is an area of engineered quantum systems in which a mechanical resonator and an electromagnetic mode form a coupled-oscillator system [4]. Although the intrinsic coupling rate between single photons and phonons is typically small, cavity optomechanical systems allow an enhancement of the coupling proportional to the amplitude of a coherent cavity drive. This parametric enhancement has allowed demonstrations of strong coupling both at ambient temperatures [5, 6] and in cryogenic, quantum-coherent regimes [7–10]. In practice, as the intensity of the coherent drive becomes large, it can induce other undesirable effects including heating and cavity nonlinearity, limiting the final parametric coupling. Operating deeply within the quantum-coherent ultrastrong coupling regime therefore requires a dramatic increase in either the single-photon optomechanical coupling rate or the cavity's power handling capability. Specifically, in the

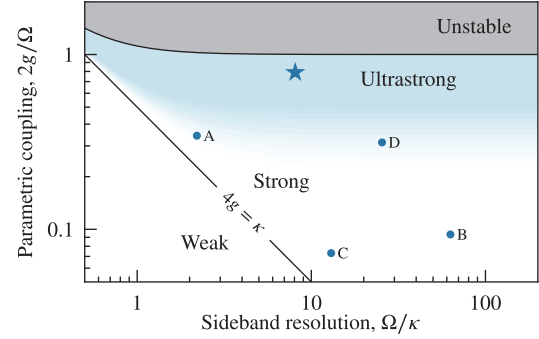


FIG. 1. Parameter space diagram showing four regimes of parametric optomechanical coupling g as a function of cavity dissipation κ and mechanical frequency Ω . For a parametric drive at $\Delta = -\Omega$, strong coupling coincides with the normal-mode splitting condition $\kappa < 4g$. Ultrastrong coupling arises when g further increases to a significant fraction of Ω until reaching the limit for stability at $2g = \sqrt{\Omega^2 + \kappa^2}/4$. Labeled points denote previous optomechanical experiments in the strong coupling regime: (A) optical Fabry-Pérot cavity [5], (B) lumped element microwave circuit [7], (C) toroidal optical microcavity [8], and (D) microwave loop-gap cavity [9]. The star indicates the highest coupling rate achieved in this work.

microwave domain, one prominent optomechanical platform is a lumped element superconducting circuit formed from a mechanically compliant vacuum-gap capacitor shunted by a thin-film inductor. While this architecture has enabled strong coupling [7], ground state cooling [11], and entanglement [12], the coupling rate has remained well below the onset of ultrastrong coupling effects, limited by unwanted nonlinearity of the superconducting inductor [13].

In this Letter, we introduce a new optomechanical architecture that mitigates the nonideality of previous designs, allowing us to reach ultrastrong coupling and approach the fundamental stability limit of the pure optomechanical interaction [14]. Our device consists of a microfabricated vacuum-gap capacitor embedded in a three-dimensional superconducting microwave cavity, analogous to recent work in the field of circuit quantum electrodynamics [15] and similar to other optomechanical demonstrations [9, 16–18]. Our device takes advantage of the

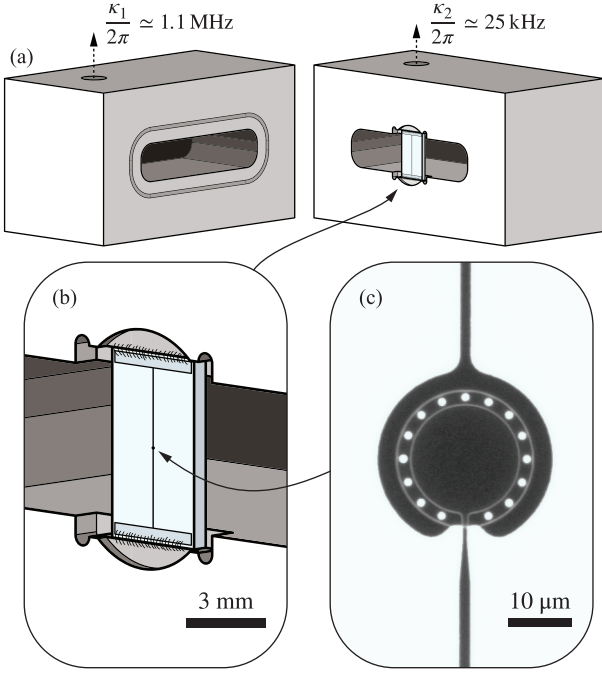


FIG. 2. Device schematic. (a) A cavity, milled from two aluminum blocks, supports a microwave resonance near 12 GHz. Microwave signals couple in and out of the cavity through two asymmetrically coupled ports. (b) An aluminum mechanically compliant capacitor patterned on a sapphire substrate is galvanically connected to the cavity walls through superconducting wirebonds, loading the fundamental cavity resonance frequency down to 6.5 GHz. (c) A micrograph image shows the capacitor, which has a fundamental mechanical resonance at 9.7 MHz and a vacuum gap of approximately 30 nm.

superior power handling of bulk cavity resonators compared to thin-film inductors. In general, the drawback of using a cavity resonator is a larger parasitic capacitance that would dilute the optomechanical coupling. Crucially, through careful microwave design and simulation, we maintain the relatively large single-photon coupling of lumped element vacuum-gap circuits [7]. As a result, we achieve ultrastrong parametric coupling by applying microwave drives with one hundred times larger power, ultimately limited by the instability inherent in the optomechanical Hamiltonian. Due to the low temperature operation, the quantum decoherence rates are kept sufficiently small to enable new regimes of entanglement [14, 19], nonlinear quantum optomechanics [20], and ultrafast quantum state transfer [21–23].

In a generic cavity optomechanical system, the natural frequency ω_c of an electromagnetic resonance depends on the position \hat{x} of a mechanical harmonic oscillator [4]. The interaction Hamiltonian is $\hat{H}_{\text{int}} = \hbar g_0 \hat{n} \hat{x} / x_{zp}$, where g_0 is the single-photon coupling rate, \hat{n} is the number operator for microwave photons, and \hbar is the reduced Planck constant. $x_{zp} = \sqrt{\hbar / 2m\Omega}$ is the mechanical zero-point fluctuation amplitude, where m and Ω are the effective mass and the resonance frequency of the mechanical mode, respectively. Dissipation in the system is characterized by damping rates κ for the electrical mode and

Γ for the mechanical mode, with $\Gamma \ll \kappa$. Even if g_0 is small, as is the case in most optomechanical systems, the coupling can be parametrically enhanced by driving the electrical mode to a coherent state of mean photon number n_d at frequency ω_d . Defining \hat{a} as the annihilation operator for fluctuations around the driven state, we can approximate the interaction Hamiltonian as $\hat{H}_{\text{int}} = \hbar g (\hat{a} + \hat{a}^\dagger) \hat{x} / x_{zp}$, where $g = g_0 \sqrt{n_d}$ is the parametrically enhanced coupling rate, leading to a set of linear coupled equations of motion for $\hat{a}(t)$ and $\hat{x}(t)$. Just as two passively coupled oscillators interact most strongly when resonant with each other, for parametric coupling an effective resonance condition is reached when driving the system at the difference frequency ($\Delta \equiv \omega_d - \omega_c = -\Omega$) in the resolved sideband regime ($\kappa \ll \Omega$). These conditions optimize the coherent exchange of energy between the mechanical and electromagnetic modes.

As the driven coupling g is increased from its small single-photon value, we encounter several distinct regimes of coupling. When the cooperativity $C = 4g^2 / \kappa\Gamma$ reaches 1, the optical damping of the mechanical mode begins to dominate over its intrinsic dissipation. As g increases further, the effective mechanical linewidth increases until it reaches the cavity dissipation rate when $g = \kappa/4$. Above this threshold, the system enters the strong-coupling regime where the cavity and mechanical mode hybridize, with the mechanical resonance frequency splitting into two solutions, which for $g \ll \Omega$ are given by

$$\Omega_{\pm} \simeq \Omega \pm \sqrt{g^2 - \kappa^2/16}. \quad (1)$$

This leads to the splitting frequency $\Omega_s = \Omega_+ - \Omega_- \simeq 2g$ when the coupling overwhelms the cavity dissipation. In this regime of strong coupling, the two physical resonators exchange energy and information at a rate Ω_s , faster than any dissipation in the system.

As the splitting frequency Ω_s approaches the bare mechanical frequency Ω , however, counter-rotating terms of order g/Ω cannot be ignored, requiring the use of the exact eigenfrequency spectrum [24]

$$\Omega_{\pm} = \text{Re} \sqrt{\Omega^2 - \frac{\kappa^2}{16} \pm 2\Omega \sqrt{g^2 - \frac{\kappa^2}{16}}}. \quad (2)$$

The discrepancy between (1) and (2) is a measurable metric to distinguish strong and ultrastrong parametric coupling. In the resolved sideband ultrastrong coupling regime ($\kappa \ll 2g < \Omega$), Eq. (2) becomes $\Omega_{\pm} \simeq \Omega \sqrt{1 \pm 2g/\Omega}$, showing that the splitting exceeds $2g$ until the system becomes parametrically unstable when $\Omega_- = 0$ at $g = \Omega/2$, corresponding to a splitting frequency $\Omega_s = \sqrt{2}\Omega$.

The regimes discussed above are shown in Fig. 1 as a function of parametric coupling and sideband resolution Ω/κ . The shaded region of ultrastrong coupling corresponds to $\Omega/5 < \Omega_s$, roughly where terms of order g/Ω become relevant while still satisfying the condition for strong coupling. As Ω_s characterizes the rate at which the two physical resonators exchange

energy, the instability sets a fundamental limit for both optomechanical coupling as well as coherent exchange of information between the resonators in the steady state. Reaching ultrastrong coupling therefore allows the exploration of the fundamental limitations of coupling in optomechanical systems.

For quantum applications, the coupling rate should be compared not only to dissipation but also to the decoherence rates in the system. In particular, the mechanical thermal decoherence rate $n_{\text{th}}\Gamma$ can be much larger than the intrinsic dissipation Γ , where n_{th} is the mechanical occupancy when in equilibrium with its thermal environment. Ideally, the quantum cooperativity $C_q = 4g^2/\kappa n_{\text{th}}\Gamma$ exceeds 1 before the onset of strong coupling, ensuring that the hybridized system is quantum coherent. In the following, we present an optomechanical device that achieves the hierarchy of rates desired for quantum coherent ultrastrong coupling: $n_{\text{th}}\Gamma \ll \kappa/2 \ll 2g \lesssim \Omega \ll \omega_c$.

Our device is shown in Fig. 2. A microwave cavity resonator with inner dimensions $19 \text{ mm} \times 4 \text{ mm} \times 17 \text{ mm}$ milled from bulk aluminum defines the electrical resonance of the system. We focus on the fundamental TE_{101} microwave mode, whose electric field is maximal at the center of the cavity, where we place a sapphire chip containing a microfabricated $20 \mu\text{m}$ -diameter aluminum vacuum-gap capacitor [22]. The suspended top plate of the capacitor forms the mechanical resonator of the system. Reducing the parasitic capacitance of the cavity and thereby maximizing the optomechanical coupling rate requires a galvanic connection between the microfabricated capacitor and the cavity walls. To achieve this, we use aluminum bond wires to connect the cavity faces to lithographically patterned pads, which then connect to the capacitor through thin-film aluminum wires.

The vacuum-gap capacitor and sapphire substrate load the cavity resonance, pulling its frequency from around 12 GHz down to $\omega_c/2\pi \approx 6.506 \text{ GHz}$. Two cavity ports with adjustable coupling pins allow signals to couple in and out to coaxial cables. We adjust the length of the pins at room temperature so the two ports contribute asymmetrically to the total dissipation $\kappa = \kappa_1 + \kappa_2 + \kappa_i$, where $\kappa_1/2\pi \approx 1.1 \text{ MHz}$ and $\kappa_2/2\pi \approx 25 \text{ kHz}$ are the port coupling rates. The internal dissipation κ_i of the cavity mode ranges from $\sim 30 \text{ kHz}$ to $\sim 140 \text{ kHz}$ depending on the circulating power [25]. The cavity is therefore overcoupled with a total dissipation rate $\kappa/2\pi \approx 1.2 \text{ MHz}$. We place the device in a cryostat with a base temperature of 16 mK and probe and monitor the system with microwave signals applied near the cavity resonance frequency. Our setup allows us to measure all four elements of the scattering matrix for a broad range of parametric coupling parameters. With a weak cavity drive, we characterize the fundamental vibrational mode of the capacitor plate by its resonance frequency $\Omega/2\pi = 9.696 \text{ MHz}$ and its intrinsic damping rate $\Gamma/2\pi = (31 \pm 1) \text{ Hz}$, measured spectroscopically, where the uncertainty represents the standard error of the mean. By varying the cryostat temperature and measuring mechanical thermal noise, we determine the single-photon optomechanical coupling rate $g_0/2\pi = (167 \pm 2) \text{ Hz}$ [11]. We also find that at base temperature, the mechanical mode equilibrates to $(35 \pm 3) \text{ mK}$, corresponding to a thermal

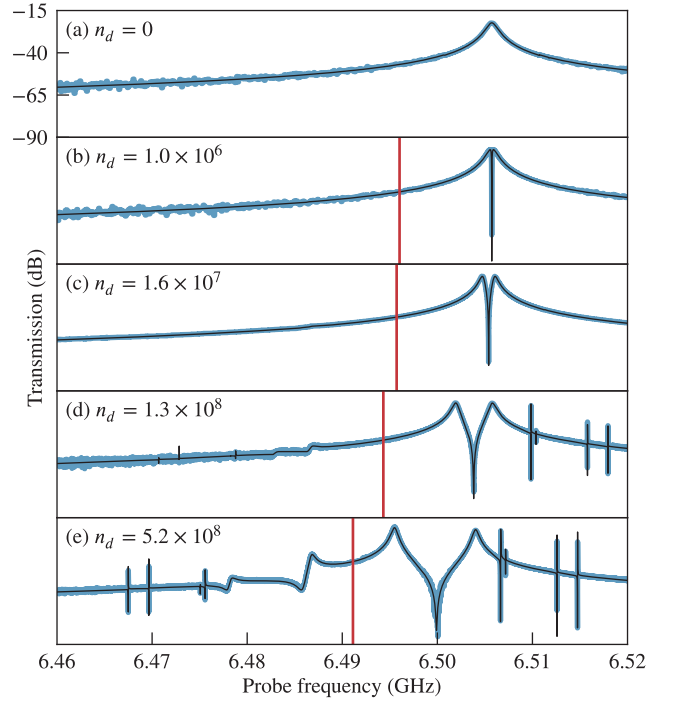


FIG. 3. Measured and calibrated cavity transmission from port one to port two for varied drive strengths n_d from weak through strong coupling and up to ultrastrong coupling. The data (blue) is fit to theory (black) containing the first five mechanical modes. The vertical red line indicates the frequency of the applied microwave drive, which is adjusted with power to maintain $\Delta = -\Omega$. The structure below the drive frequency at the highest powers directly shows the importance of counter-rotating terms in the ultrastrong coupling regime.

phonon occupancy $n_{\text{th}} = 76 \pm 6$.

To probe the response of the coupled system, we measure the vector transmission of the microwave field through the cavity in the presence of a parametric drive [7, 26, 27]. In Fig. 3, we plot the magnitude of the transmission for a range of drive powers applied below the cavity resonance, with the drive frequency indicated as a red vertical line. We coherently cancel the drive after it leaves the cavity, allowing us to measure the transmission of a weak probe without saturating our microwave measurement [24]. We adjust the drive frequency as we increase drive power to maintain the condition $\Delta = -\Omega$ in the presence of two dominant nonlinear effects. Namely, we measure the pure optomechanical Kerr shift, $-2g_0^2/\Omega = (-5.8 \pm 0.1) \text{ mHz/photon}$, and we attribute the remaining shift to the residual nonlinear kinetic inductance of the superconducting film, approximately -4 mHz/photon at our highest powers [13].

At low drive power (Fig. 3a), we measure the bare cavity resonance, a single Lorentzian with linewidth κ . As the drive power increases (Fig. 3b), the optomechanical interaction appears as interference in the cavity response with a characteristic bandwidth of the damped mechanical linewidth $\sim 4g^2/\kappa$. At large enough power (Fig. 3c), the damped mechanical width reaches $\kappa/2$, after which the response splits into normal modes,

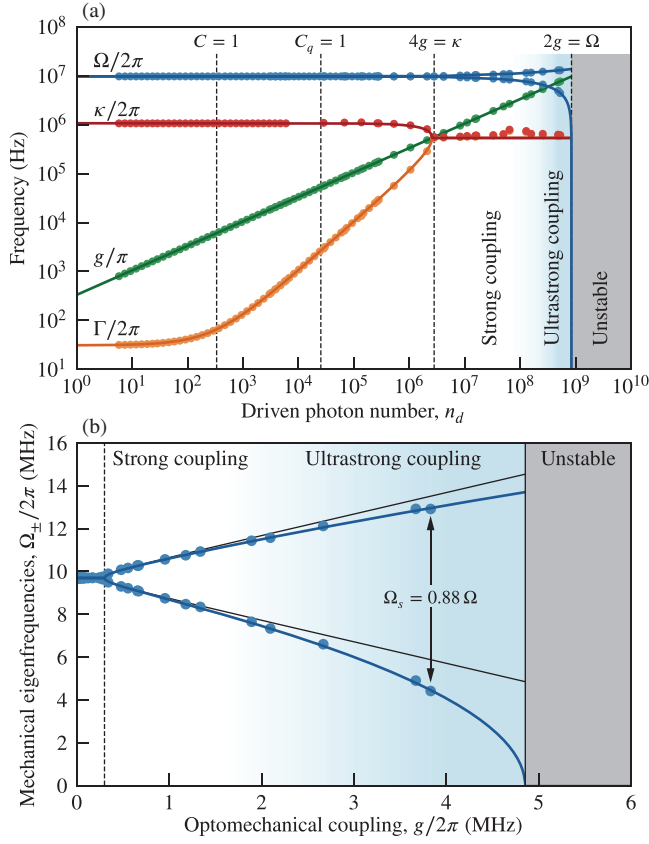


FIG. 4. (a) Measured system rates as a function of drive strength. In the weak coupling regime, the optical damping first exceeds the mechanical dissipation rate ($C = 1$) and then exceeds the thermal decoherence rate ($C_q = 1$). Once $2g$ reaches $\kappa/2$, the eigenmodes split, indicating the onset of strong coupling. Eventually, ultrastrong coupling corrections become important before the system approaches a parametric instability at $2g = \Omega$. (b) Mechanical eigenfrequencies as a function of the optomechanical coupling rate. In the ultrastrong coupling regime, the splitting $\Omega_s = \Omega_+ - \Omega_-$ exceeds the linear strong-coupling approximation $\Omega_s \simeq 2g$ (black), reaching a maximal value $\Omega_s \approx 0.88 \Omega$.

marking the strong coupling regime. Additionally, we begin to resolve the next four vibrational modes of the membrane (Fig. 3d), which couple weakly to the cavity mode. At the highest power (Fig. 3e), the response acquires several features indicative of ultrastrong coupling. In addition to the splitting of the fundamental resonance becoming of order Ω , the counter-rotating dynamics below the drive frequency become significant and easily observable. Lastly, the transmission at the drive frequency begins to increase, signifying a nonlinear relationship between input power and driven photon number in the cavity.

We fit the data in the complex plane to multimode optomechanical theory [24], shown as a black line plotted over the data. The quantitative agreement between data and theory allows us to extract all the relevant system parameters as a function of drive power. These parameters are shown in Fig. 4a from very weak parametric coupling to the ultrastrong coupling regime. For very few drive photons (in this case $n_d \lesssim 10^2$), the bare

mode properties are measured. As the drive power increases within the regime of weak coupling ($n_d \lesssim 10^6$), the mechanical mode is damped and cooled, passing through $C = 1$ and entering the quantum-enabled regime $C_q > 1$, where the occupancy is reduced below one quantum. Normal-mode splitting occurs at $n_d \approx 3 \times 10^6$ where $4g = \kappa$, marking the beginning of strong coupling. Above $n_d \approx 2 \times 10^8$, the splitting starts to deviate from $2g$ as the system enters the ultrastrong coupling regime. The threshold for parametric oscillation occurs at $n_d \approx 8.4 \times 10^8$, above which no steady-state solution exists. We measure well into the regime where $\Omega_- < 2g < \Omega_s$; that is, the energy swapping rate exceeds $2g$ as well as the lower eigenfrequency itself.

In Fig. 4b, the measured mechanical eigenfrequencies (blue circles) are plotted versus the optomechanical coupling rate. The black line shows the strong-coupling approximation (1), while the full solution (2) is shown as a blue line. The discrepancy between the two is a clear indication of ultrastrong coupling effects. At the highest power, the splitting between the two modes exceeds the frequency of the lower mode, reaching 88% of the bare mechanical frequency.

Our measurements of the driven cavity response allow us to reconstruct the mechanical susceptibility, defined as the ratio of induced motion to external force $\chi_m(\omega) = m\Omega^2 x(\omega)/F(\omega)$, normalized by the intrinsic mechanical spring constant $m\Omega^2$. This is shown in Fig. 5. The gray line corresponds to the estimated susceptibility at zero coupling, which includes the bare resonance of the fundamental mode as well as the first four higher-order vibrational modes. The peak height on resonance is equal to the quality factor of the fundamental mode, $Q_m = \Omega/\Gamma \approx 3 \times 10^5$, while the heights at the other resonances are reduced due to their lower vacuum coupling rates. The data plotted in blue (with a fit to theory in black) is the susceptibility inferred from our highest drive power in Fig. 3. The original peak of linewidth Γ is split into two broad peaks with approximate widths $\kappa/2$, each representing a normal mode of the joint cavity-mechanics system. At this large coupling rate, the eigenfrequencies are no longer split symmetrically about the bare mechanical frequency, and the peak heights are unequal. As the lower eigenfrequency decreases, we also see an increase in the value of susceptibility at zero frequency, indicating an increased response to static forces. All of these effects agree with the full optomechanical theory that includes ultrastrong-coupling corrections. At our highest cooperativity of $C \approx 1.6 \times 10^6$, we achieve a maximal splitting of $\Omega_s/2\pi \approx 8.5$ MHz. Here, the state of the mechanical mode is exchanged with the cavity mode in a characteristic time $\pi/\Omega_s \approx 60$ ns, faster than the mechanical oscillation period $2\pi/\Omega \approx 100$ ns.

In conclusion, we have introduced a novel microwave optomechanical circuit architecture and experimentally characterized the eigenmodes of the system in the quantum regime. As the parametric coupling is increased *in situ*, we find quantitative agreement with the theoretical predictions from weak to ultrastrong coupling. Looking forward, ultrastrong coupling of bosonic modes is predicted to have interesting ground state properties [28–31]. Quantum correlations induced by the

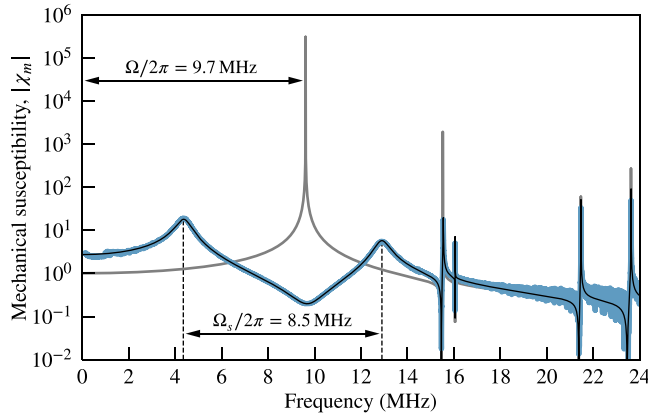


FIG. 5. Mechanical susceptibility inferred from microwave measurements at our highest drive power (blue) with fit line (black) compared with the bare susceptibility (gray). In agreement with the full theory, the susceptibility in the ultrastrong coupling regime shows asymmetry at the two eigenfrequencies as well as a marked increase in its value at zero frequency. Here, the splitting is 8.5 MHz with a corresponding cooperativity of $C \approx 1.6 \times 10^6$.

counter-rotating terms in the ultrastrong coupling regime induce squeezing and entanglement between the mechanical and cavity modes [19]. Studying the noise properties in this regime would also allow us to observe these effects for the first time, as well as assess how these correlations could be exploited for quantum-enhanced sensing of forces, displacements, or gravitational waves [32–34]. Furthermore, while the fundamental instability precludes traditional steady-state measurements when the swapping rate exceeds the mechanical frequency, pulsed measurements would allow the system to be characterized beyond this limit into the deep strong coupling regime [2, 3]. These ultrafast pulsed measurements would allow new regimes of quantum state transfer [21, 23], entanglement [12], topologically-protected operations [35], and projective measurements [36]. Finally, theoretical proposals have suggested using ultrastrong coupling to enhance the weak nonlinear terms of the optomechanical Hamiltonian [20] allowing for nonlinear quantum optomechanics.

G. A. Peterson acknowledges support from the National Physical Science Consortium. Official contribution of the National Institute of Standards and Technology; not subject to copyright in the United States.

- [1] H. Mabuchi and A. C. Doherty, “Cavity quantum electrodynamics: Coherence in context,” *Science* **298**, 1372–1377 (2002).
- [2] A. F. Kockum, A. Miranowicz, S. De Liberato, S. Savasta, and F. Nori, “Ultrastrong coupling between light and matter,” *Nat. Rev. Phys.* **1**, 19–40 (2019).
- [3] P. Forn-Díaz, L. Lamata, E. Rico, J. Kono, and E. Solano, “Ultrastrong coupling regimes of light-matter interaction,” *Rev. Mod. Phys.* **91**, 025005 (2019).
- [4] M. Aspelmeyer, T. J. Kippenberg, and F. Marquardt, “Cavity

- optomechanics,” *Rev. Mod. Phys.* **86**, 1391–1452 (2014).
- [5] S. Gröblacher, K. Hammerer, M. R. Vanner, and M. Aspelmeyer, “Observation of strong coupling between a micromechanical resonator and an optical cavity field,” *Nature (London)* **460**, 724–727 (2009).
- [6] G.ENZIAN, M. Szczykulska, J. Silver, L. Del Bino, S. Zhang, I. A. Walmsley, P. Del’Haye, and M. R. Vanner, “Observation of Brillouin optomechanical strong coupling with an 11 GHz mechanical mode,” *Optica* **6**, 7–14 (2019).
- [7] J. D. Teufel, D. Li, M. S. Allman, K. Cicak, A. J. Sirois, J. D. Whittaker, and R. W. Simmonds, “Circuit cavity electromechanics in the strong-coupling regime,” *Nature (London)* **471**, 204–208 (2011).
- [8] E. Verhagen, S. Deléglise, S. Weis, A. Schliesser, and T. J. Kippenberg, “Quantum-coherent coupling of a mechanical oscillator to an optical cavity mode,” *Nature (London)* **482**, 63–67 (2012).
- [9] A. Noguchi, R. Yamazaki, M. Ataka, H. Fujita, Y. Tabuchi, T. Ishikawa, K. Usami, and Y. Nakamura, “Ground state cooling of a quantum electromechanical system with a silicon nitride membrane in a 3D loop-gap cavity,” *New J. Phys.* **18**, 103036 (2016).
- [10] P. Kharel, Y. Chu, E. A. Kittlaus, N. T. Otterstrom, S. Gertler, and P. T. Rakich, “Multimode strong coupling in cavity optomechanics,” *arXiv* **18**, 1812.06202 (2018).
- [11] J. D. Teufel, T. Donner, D. Li, J. W. Harlow, M. S. Allman, K. Cicak, A. J. Sirois, J. D. Whittaker, K. W. Lehnert, and R. W. Simmonds, “Sideband cooling of micromechanical motion to the quantum ground state,” *Nature (London)* **475**, 359–363 (2011).
- [12] T. A. Palomaki, J. D. Teufel, R. W. Simmonds, and K. W. Lehnert, “Entangling mechanical motion with microwave fields,” *Science* **342**, 710–713 (2013).
- [13] J. Zmuidzinas, “Superconducting microresonators: Physics and applications,” *Annu. Rev. Condens. Matter Phys.* **3**, 169–214 (2012).
- [14] S. Aldana, C. Bruder, and A. Nunnenkamp, “Equivalence between an optomechanical system and a Kerr medium,” *Phys. Rev. A* **88**, 043826 (2013).
- [15] H. Paik, D. I. Schuster, L. S. Bishop, G. Kirchmair, G. Catelani, A. P. Sears, B. R. Johnson, M. J. Reagor, L. Frunzio, L. I. Glazman, S. M. Girvin, M. H. Devoret, and R. J. Schoelkopf, “Observation of high coherence in Josephson junction qubits measured in a three-dimensional circuit QED architecture,” *Phys. Rev. Lett.* **107**, 240501 (2011).
- [16] M. E. Tobar and D. G. Blair, “Parametric transducers for resonant bar gravitational wave antennae,” *J. Phys. D: Appl. Phys.* **26**, 2276 (1993).
- [17] M. Yuan, V. Singh, Y. M. Blanter, and G. A. Steele, “Large cooperativity and microkelvin cooling with a three-dimensional optomechanical cavity,” *Nat. Commun.* **6**, 8491 (2015).
- [18] B. Gunupudi, S. R. Das, R. Navarathna, S. K. Sahu, S. Majumder, and V. Singh, “An optomechanical platform with a three-dimensional waveguide cavity,” *Phys. Rev. Appl.* **11**, 024067 (2019).
- [19] S. G. Hofer and K. Hammerer, “Entanglement-enhanced time-continuous quantum control in optomechanics,” *Phys. Rev. A* **91**, 033822 (2015).
- [20] M.-A. Lemonde, N. Didier, and A. A. Clerk, “Nonlinear interaction effects in a strongly driven optomechanical cavity,” *Phys. Rev. Lett.* **111**, 053602 (2013).
- [21] T. A. Palomaki, J. W. Harlow, J. D. Teufel, R. W. Simmonds, and K. W. Lehnert, “Coherent state transfer between itinerant microwave fields and a mechanical oscillator,” *Nature (London)* **495**, 210–214 (2013).
- [22] F. Lecocq, J. D. Teufel, J. Aumentado, and R. W. Simmonds,

- “Resolving the vacuum fluctuations of an optomechanical system using an artificial atom,” *Nat. Phys.* **11**, 635–639 (2015), see supplementary information.
- [23] A. P. Reed, K. H. Mayer, J. D. Teufel, L. D. Burkhardt, W. Pfaff, M. Reagor, L. Sletten, X. Ma, R. J. Schoelkopf, E. Knill, and K. W. Lehnert, “Faithful conversion of propagating quantum information to mechanical motion,” *Nat. Phys.* **13**, 1163–1167 (2017).
- [24] See supplementary information.
- [25] J. M. Martinis, K. B. Cooper, R. McDermott, M. Steffen, M. Ansmann, K. D. Osborn, K. Cicak, S. Oh, D. P. Pappas, R. W. Simmonds, and C. C. Yu, “Decoherence in josephson qubits from dielectric loss,” *Phys. Rev. Lett.* **95**, 210503 (2005).
- [26] S. Weis, R. Rivière, S. Deléglise, E. Gavartin, O. Arcizet, A. Schliesser, and T. J. Kippenberg, “Optomechanically induced transparency,” *Science* **330**, 1520 (2010).
- [27] A. H. Safavi-Naeini, T. P. Mayer Alegre, J. Chan, M. Eichenfield, M. Winger, Q. Lin, J. T. Hill, D. E. Chang, and O. Painter, “Electromagnetically induced transparency and slow light with optomechanics,” *Nature (London)* **472**, 69–73 (2011).
- [28] C. Ciuti, G. Bastard, and I. Carusotto, “Quantum vacuum properties of the intersubband cavity polariton field,” *Phys. Rev. B* **72**, 115303 (2005).
- [29] C. Ciuti and I. Carusotto, “Input-output theory of cavities in the ultrastrong coupling regime: The case of time-independent cavity parameters,” *Phys. Rev. A* **74**, 033811 (2006).
- [30] S. Fedortchenko, S. Felicetti, D. Marković, S. Jezouin, A. Keller, T. Coudreau, B. Huard, and P. Milman, “Quantum simulation of ultrastrongly coupled bosonic modes using superconducting circuits,” *Phys. Rev. A* **95**, 042313 (2017).
- [31] D. Marković, S. Jezouin, Q. Ficheux, S. Fedortchenko, S. Felicetti, T. Coudreau, P. Milman, Z. Leghtas, and B. Huard, “Demonstration of an effective ultrastrong coupling between two oscillators,” *Phys. Rev. Lett.* **121**, 040505 (2018).
- [32] R. Schnabel, N. Mavalvala, D. E. McClelland, and P. K. Lam, “Quantum metrology for gravitational wave astronomy,” *Nat. Commun.* **1**, 121 (2010).
- [33] N. S. Kampel, R. W. Peterson, R. Fischer, P.-L. Yu, K. Cicak, R. W. Simmonds, K. W. Lehnert, and C. A. Regal, “Improving broadband displacement detection with quantum correlations,” *Phys. Rev. X* **7**, 021008 (2017).
- [34] D. Mason, J. Chen, M. Rossi, Y. Tsaturyan, and A. Schliesser, “Continuous force and displacement measurement below the standard quantum limit,” *Nat. Phys.* (2019), 10.1038/s41567-019-0533-5.
- [35] H. Xu, D. Mason, L. Jiang, and J. G. E. Harris, “Topological energy transfer in an optomechanical system with exceptional points,” *Nature (London)* **537**, 80–83 (2016).
- [36] M. R. Vanner, I. Pikovski, G. D. Cole, M. S. Kim, Č. Brukner, K. Hammerer, G. J. Milburn, and M. Aspelmeyer, “Pulsed quantum optomechanics,” *Proc. Nat. Acad. Sci. USA* **108**, 16182–16187 (2011).

SUPPLEMENTARY INFORMATION

Ultrastrong parametric coupling between a superconducting cavity and a mechanical resonator

G. A. Peterson,^{1,2} S. Kotler,^{1,2} F. Lecocq,^{1,2} K. Cicak,¹ X. Y. Jin,^{1,2}
R. W. Simmonds,¹ J. Aumentado,¹ and J. D. Teufel¹

¹*National Institute of Standards and Technology, 325 Broadway, Boulder, CO 80305, USA*

²*Department of Physics, University of Colorado, Boulder, CO 80309, USA*

1 Derivation of optomechanical interactions in the ultrastrong coupling regime

The Hamiltonian for a cavity optomechanical system is [1]

$$\hat{H} = \hbar\omega_c(\hat{x})\left(\hat{n} + \frac{1}{2}\right) + \frac{\hat{p}^2}{2m} + \frac{1}{2}m\Omega^2\hat{x}^2, \quad (\text{S1})$$

where ω_c and \hat{n} are the resonance frequency and number operator for the microwave cavity mode, and \hat{p} , m , Ω , and \hat{x} are the momentum, effective mass, resonance frequency, and position of the mechanical harmonic oscillator. The cavity frequency's dependence on mechanical position gives rise to optomechanical coupling. For small mechanical fluctuations, we use $\omega_c(\hat{x}) = \omega_c - g_0\hat{x}/x_{zp}$, where g_0 is the single-photon coupling rate and $x_{zp} = \sqrt{\hbar/2m\Omega}$ is the mechanical zero-point fluctuation amplitude, giving rise to the interaction Hamiltonian in the main text: $\hat{H}_{\text{int}} = \hbar g_0 \hat{n} \hat{x}/x_{zp}$.

In the presence of a strong cavity drive at frequency $\omega_d = \omega_c + \Delta$, the cavity mode becomes populated with a coherent state of n_d driven photons. We expand the Hamiltonian to first order in the fluctuations \hat{a} around this driven coherent state using $\hat{n} = (\sqrt{n_d}e^{i\omega_d t} + \hat{a}^\dagger)(\sqrt{n_d}e^{-i\omega_d t} + \hat{a}) \simeq n_d + \sqrt{n_d}(\hat{a}^\dagger e^{-i\omega_d t} + \hat{a}e^{i\omega_d t})$. With $g = g_0\sqrt{n_d}$ as the parametric coupling, the interaction Hamiltonian becomes

$$\hat{H}_{\text{int}} = \hbar g_0 n_d \hat{x}/x_{zp} + \hbar g (\hat{a}^\dagger e^{-i\omega_d t} + \hat{a}e^{i\omega_d t}) \hat{x}/x_{zp}. \quad (\text{S2})$$

The first term represents a static radiation pressure force that pulls the capacitor plates closer together. This leads to a power-dependent shift of the equilibrium position by $2x_{zp}g_0n_d/\Omega$ and a shift in the cavity frequency by $-2g^2/\Omega$. These shifts can be absorbed into the definitions of \hat{x} and ω_c . The linearized Heisenberg–Langevin equations of motion are then given by

$$\ddot{\hat{x}} + \Gamma\dot{\hat{x}} + \Omega^2\hat{x} = 2\Omega x_{zp}g (\hat{a}e^{i\omega_d t} + \hat{a}^\dagger e^{-i\omega_d t}) + \frac{\hat{F}_{\text{ext}}}{m}, \quad (\text{S3})$$

$$\dot{\hat{a}} + i\left(\omega_c - \frac{\kappa}{2}\right)\hat{a} = ig\frac{\hat{x}}{x_{zp}}e^{-i\omega_d t} + \sqrt{\kappa}\hat{a}_{\text{in}}. \quad (\text{S4})$$

where we have included damping rates (κ and Γ) and external driving (\hat{a}_{in} and \hat{F}_{ext}) for each resonator. We can write these equations of motion in compact matrix form in the Fourier domain as

$$\mathbf{M}(\omega) \begin{pmatrix} \hat{a}(\omega_d + \omega) \\ \hat{x}(\omega)/x_{zp} \\ \hat{a}^\dagger(\omega_d - \omega) \end{pmatrix} = \begin{pmatrix} i\sqrt{\kappa_{\text{ext}}}\hat{a}_{\text{in}}(\omega_d + \omega) \\ \hat{F}_{\text{ext}}(\omega)/2p_{zp} \\ i\sqrt{\kappa_{\text{ext}}}\hat{a}_{\text{in}}^\dagger(\omega_d - \omega) \end{pmatrix}, \quad (\text{S5})$$

where $p_{zp} = \sqrt{\hbar m \Omega}/2$ is the zero-point momentum and the mode-coupling matrix is

$$\mathbf{M}(\omega) = \begin{pmatrix} \chi_a^{-1}(\omega_d + \omega) & g & 0 \\ g & \chi_x^{-1}(\omega) & g \\ 0 & -g & -\chi_a^{-1}(\omega_d - \omega)^* \end{pmatrix}, \quad (\text{S6})$$

where

$$\chi_a(\omega) = 1/(\omega - \omega_c + i\kappa/2), \quad (\text{S7})$$

$$\chi_x(\omega) = 2\Omega/(\omega^2 - \Omega^2 + i\omega\Gamma), \quad (\text{S8})$$

are the complex susceptibility functions for the cavity and mechanical mode, respectively.

We model the cavity transmission as $T(\omega) = i\sqrt{\kappa_1\kappa_2}\chi_{a,\text{eff}}(\omega)$, where $\chi_{a,\text{eff}} \equiv (\mathbf{M}^{-1})_{11}$ is the effective cavity susceptibility in the presence of optomechanical coupling, given by

$$\chi_{a,\text{eff}}(\omega) = \left[\chi_a^{-1}(\omega) - \frac{g^2}{\chi_x^{-1}(\omega - \omega_d) - g^2\chi_a^*(2\omega_d - \omega)} \right]^{-1}. \quad (\text{S9})$$

Similarly, the effective mechanical susceptibility $\chi_{x,\text{eff}} \equiv (\mathbf{M}^{-1})_{22}$ is given by

$$\chi_{x,\text{eff}}(\omega) = \left[\chi_x^{-1}(\omega) - g^2\chi_a(\omega_d + \omega) - g^2\chi_a^*(\omega_d - \omega) \right]^{-1}. \quad (\text{S10})$$

In the main text, we discuss the normalized effective mechanical susceptibility $\chi_m = \Omega\chi_{x,\text{eff}}/2$, such that χ_m is dimensionless with a value of Q_m on resonance. The mechanical displacement due to a radiation-pressure force F is then $x(\omega) = \chi_m(\omega)F(\omega)/m\Omega^2$. A measurement of the cavity transmission $T(\omega)$ allows us to extract the mechanical susceptibility from

$$\chi_m(\omega - \omega_d) = \frac{\Omega}{2g^2\chi_a(\omega)} \left(\frac{T(\omega)}{i\sqrt{\kappa_1\kappa_2}\chi_a(\omega)} - 1 \right). \quad (\text{S11})$$

Accounting for multiple mechanical modes is straightforward and relevant for modeling our data. We assume there are N mechanical modes, each with a susceptibility χ_i , which contains the mode's resonance frequency and linewidth as in Eq. (S8), and a parametric coupling rate g_i . The extra modes modify the effective cavity susceptibility (S9)

such that χ_x is replaced by a sum over the mechanical mode susceptibilities, weighted by their coupling rates: $\chi_x \rightarrow \chi_{xN}$, where

$$\chi_{xN}(\omega) = \sum_{i=1}^N \left(\frac{g_i}{g_1} \right)^2 \chi_i(\omega). \quad (\text{S12})$$

This weighted sum is therefore the effective multimode mechanical susceptibility to radiation pressure forces. To perform calculations that account for the higher order modes, we simply replace χ_x in the above discussion with χ_{xN} .

To understand normal-mode splitting and stability, we calculate the eigenvalues of the optomechanical equations of motion. These are given by the zeros of the determinant of the mode-coupling matrix: $|\mathbf{M}(\lambda)| = 0$.

$$0 = \left(\frac{\lambda^2 - \Omega^2 + i\Gamma\lambda}{2\Omega} \right) \left(\lambda - \Delta + \frac{i\kappa}{2} \right) \left(\lambda + \Delta + \frac{i\kappa}{2} \right) + 2\Delta g^2. \quad (\text{S13})$$

For $\Delta = -\Omega$, the four solutions are

$$\lambda_{\pm\pm} = \frac{\kappa + \Gamma}{4i} \pm \sqrt{\Omega^2 - \left(\frac{\kappa - \Gamma}{4} \right)^2 \pm 2\Omega \sqrt{g^2 - \left(\frac{\kappa - \Gamma}{4} \right)^2}}. \quad (\text{S14})$$

Each of the solutions has a corresponding time dependence of $e^{-i\lambda t}$, so that $\text{Re}[\lambda]$ describes the eigenmode's frequency and $\text{Im}[\lambda]$ describes its damping rate. If any of the eigenvalues has a positive imaginary part, the mode amplitude grows exponentially, and the system is said to be unstable. Using this criterion, we find that for a red-detuned drive ($\Delta < 0$), and assuming a large mechanical quality factor ($\Gamma \ll \Omega$), the optomechanical system is unstable for

$$g^2 > -\frac{\Omega}{4\Delta} \left(\Delta^2 + \frac{\kappa^2}{4} \right). \quad (\text{S15})$$

2 Supplementary data and measurements

Figure S1 shows the measured mechanical mode temperature as the cryostat temperature is varied. The data indicates that the mechanical mode thermalizes with the cryostat down to 35 mK, where it becomes thermally decoupled.

Figure S2 shows the result of a finite-element simulation of the three-dimensional microwave fields in the cavity in the presence of the sapphire substrate and a lumped element capacitor. The resonant frequency of the fundamental mode agrees well with a lumped element circuit model where the cavity mode is modeled as a parallel LC resonance, and the moving capacitor is attached through two inductors, modeling the thin-film leads in our device.

See Figure S3 for a simplified diagram of the experimental setup. Table 1 summarizes the relevant optomechanical parameters of the device.

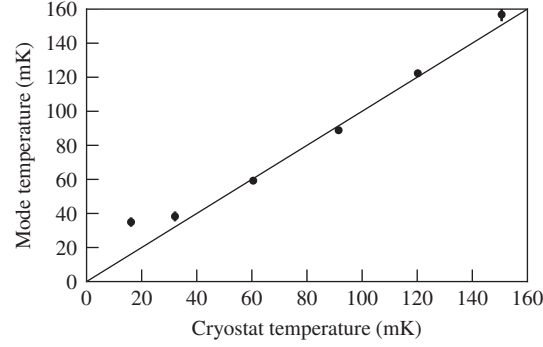


Figure S1: Measured mechanical mode temperature as the cryostat temperature is varied. The mode thermalizes to the cryostat for temperatures above around 40 mK. At base temperature, the mechanical mode reaches 35 mK.

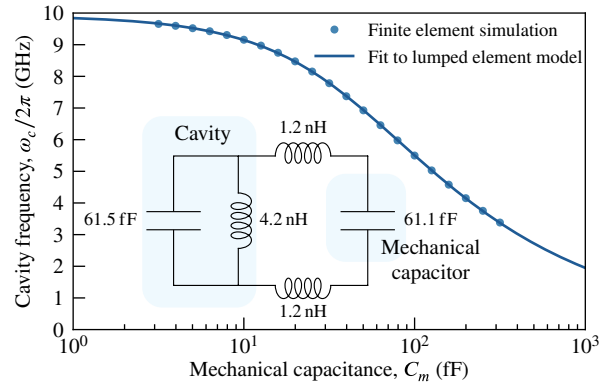


Figure S2: Comparison of a three-dimensional finite-element simulation with a lumped-element circuit model, shown in inset. The simulation solves for the electromagnetic fields in the cavity as a function of a lumped-element capacitance, taking into account the sapphire substrate and superconducting leads connecting the capacitor to the cavity walls. The inset shows the effective circuit model for our device, where the mechanical capacitance is 61.1 fF, corresponding to a parallel plate separation of 29 nm.

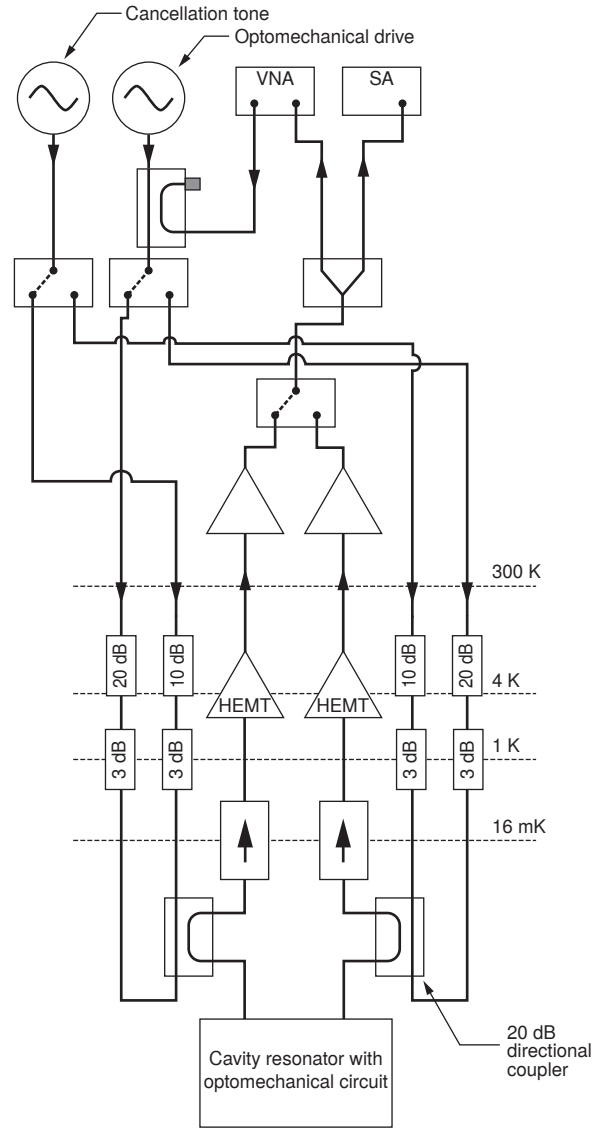


Figure S3: Simplified diagram of experimental setup. Two microwave generators and a vector network analyzer (VNA) act as microwave sources whose signals are attenuated at low temperature and delivered to the optomechanical device. The output signals are amplified by cryogenic high electron mobility transistor (HEMT) amplifiers and room temperature microwave amplifiers and then measured by the VNA and a spectrum analyzer (SA).

Table 1: Summary of system parameters.

Description	Variable	Value/ 2π	Unit
Cavity frequency	ω_c	6.506	GHz
Cavity linewidth	κ	1.2	MHz
Mechanical frequency	Ω	9.696	MHz
Mechanical linewidth	Γ	31 ± 1	Hz
Thermal decoherence rate	$n_{\text{th}}\Gamma$	2.4 ± 0.5	kHz
Single-photon coupling rate	g_0	167 ± 2	Hz
Largest coupling rate	g	3.83	MHz
Largest swapping rate	Ω_s	8.5	MHz

References

- [1] M. Aspelmeyer, T. J. Kippenberg, and F. Marquardt. Cavity optomechanics. *Rev. Mod. Phys.*, 86(4):1391–1452, 2014.